Electrical pump & probe and injected carrier losses quantification in Er doped Si slot waveguides

J. M. Ramírez,[1,*] Y. Berencén,[1] F. Ferrarese Lupi,[1] D. Navarro-Urrios,[4] A. Anopchenko,[2] A. Tengattini,[2] N. Prtljaga,[2] L. Pavesi,[2] P. Rivallin,[3] J. M. Fedeli,[3] and B. Garrido[1]

[1]*MIND-IN2UB, Departament d'Electrònica, Universitat de Barcelona, Martí i Franquès 1, Barcelona 08028, Spain*
[2]*Nanoscience Laboratory, Department of Physics, University of Trento, Via Sommarive 14, Povo 38123, Italy*
[3]*CEA, Léti, Minatec campus 17 rue des Martyrs, Grenoble 38054, France*
[4]*Catalan Institute of Nanotechnology (CIN2-CSIC), Campus UAB, edifice CM3, Bellaterra 08193, Spain*
[*]*jmramirez@el.ub.es*

Abstract: Electrically driven Er^{3+} doped Si slot waveguides emitting at 1530 nm are demonstrated. Two different Er^{3+} doped active layers were fabricated in the slot region: a pure SiO_2 and a Si-rich oxide. Pulsed polarization driving of the waveguides was used to characterize the time response of the electroluminescence (EL) and of the signal probe transmission in 1 mm long waveguides. Injected carrier absorption losses modulate the EL signal and, since the carrier lifetime is much smaller than that of Er^{3+} ions, a sharp EL peak was observed when the polarization was switched off. A time-resolved electrical pump & probe measurement in combination with lock-in amplifier techniques allowed to quantify the injected carrier absorption losses. We found an extinction ratio of 6 dB, passive propagation losses of about 4 dB/mm, and a spectral bandwidth > 25 nm at an effective d.c. power consumption of 120 μW. All these performances suggest the usage of these devices as electro-optical modulators.

OCIS codes: (130.0250) Optoelectronics; (160.5690) Rare-earth-doped materials.

References and links

1. B. Jalali and S. Fathpour, "Silicon Photonics," J. Lightwave Technol. **24**(12), 4600–4615 (2006).
2. R. Soref, "The Past, Present, and Future of Silicon Photonics," IEEE J. Sel. Top. Quantum Electron. **12**(6), 1678–1687 (2006).
3. M. Lipson, "Guiding, modulating, and emitting light on silicon-challenges and opportunities," J. Lightwave Technol. **23**(12), 4222–4238 (2005).
4. J. D. B. Bradley and M. Pollnau, "Erbium-doped integrated waveguide amplifiers and lasers," Laser Photon. Rev. **5**(3), 368–403 (2011).
5. J. Cardenas, C. B. Poitras, J. T. Robinson, K. Preston, L. Chen, and M. Lipson, "Low loss etchless Silicon photonic waveguides," Opt. Express **17**(6), 4752–4757 (2009).
6. Y. A. Vlasov, M. O'Boyle, H. F. Hamann, and S. J. McNab, "Active control of slow light on a chip with photonic crystal waveguides," Nature **438**(7064), 65–69 (2005).
7. V. R. Almeida, Q. F. Xu, C. A. Barrios, and M. Lipson, "Guiding and confining Light in void nanostructure," Opt. Lett. **29**(11), 1209–1211 (2004).
8. M. Galli, D. Gerace, A. Politi, M. Liscidini, M. Patrini, L. C. Andreani, A. Canino, M. Miritello, R. Lo Salvio, A. Irrera, and F. Priolo, "Direct evidence of light confinement and emission enhancement in active silicon-on-insulator slot waveguides," Appl. Phys. Lett. **89**, 241114 (2006).
9. K. Preston and M. Lipson, "Slot waveguides with polycrystalline silicon for electrical injection," Opt. Express **17**(3), 1527–1534 (2009).
10. H. Jayatilleka, A. Nasrollahy-Shiraz, and A. J. Kenyon, "Electrically pumped silicon waveguide light sources," Opt. Express **19**(24), 24569–24576 (2011).
11. J. M. Ramírez, F. Ferrarese Lupi, Y. Berencén, A. Anopchenko, J. P. Colonna, O. Jambois, J. M. Fedeli, L. Pavesi, N. Prtljaga, P. Rivallin, A. Tengattini, D. Navarro-Urrios, and B. Garrido, "Er-doped light emitting slot waveguides monolithically integrated in a silicon photonic chip," Nanotechnology (to be published).

#175955 - $15.00 USD Received 11 Sep 2012; revised 30 Oct 2012; accepted 1 Nov 2012; published 12 Dec 2012

12. D. Navarro-Urrios, A. Pitanti, N. Daldosso, F. Gourbilleau, R. Rizk, G. Pucker, and L. Pavesi, "Quantification of the carrier absorption losses in Si-nanocrystal rich rib waveguides at 1.54 μm," Appl. Phys. Lett. **92**, 051101 (2008).
13. T. Creazzo, B. Redding, E. Marchena, S. Shi, and D. W. Prather, "Free-carrier absorption modulation in silicon nanocrystal slot waveguides," Opt. Lett. **35**(21), 3691–3693 (2010).
14. G. M. Miller, R. M. Briggs, and H. A. Atwater, "Achieving optical gain in waveguide-confined nanocluster-sensitized erbium by pulsed excitation," J. Appl. Phys. **108**, 063109 (2010).
15. R. Sun, P. Dong, N. N. Feng, C. Y. Hong, J. Michel, M. Lipson, and L. Kimerling, "Horizontal single and multiple slot waveguides: optical transmission at λ = 1550 nm," Opt. Express **15**(26), 17967–17972 (2007).
16. D. J. DiMaria and D. W. Dong, "High current injection into SiO_2 from Si rich SiO_2 films and experimental applications," J. Appl. Phys. **51**(5), 2722–2735 (1980).
17. J. M. Ramírez, F. Ferrarese Lupi, O. Jambois, Y. Berencén, D. Navarro-Urrios, A. Anopchenko, A. Marconi, N. Prtljaga, A. Tengattini, L. Pavesi, J. P. Colonna, J. M. Fedeli and B. Garrido, "Erbium emission in MOS light emitting devices: from energy transfer to direct impact excitation," Nanotechnology **23**, 125203 (2012).
18. F. Iacona, D. Pacifici, A. Irrera, M. Miritello, G. Franzò, and F. Priolo, "Electroluminescence at 1.54 μm in Er-doped Si nanocluster-based devices," Appl. Phys. Lett. **81**, 3242 (2002).
19. A. C. Turner-Foster, M. A. Foster, J. S. Levy, C. B. Poitras, R. Salem, A. L. Gaeta, and M. Lipson, "Ultrashort free-carrier lifetime in low-loss silicon nanowaveguides," Opt. Express **18**(4), 3582–3591 (2010).
20. J. Liu, M. Beals, A. Pomerene, S. Bernardis, R. Sun, J. Cheng, L. C. Kimerling, and J. Michel, "Waveguide-integrated, ultralow-energy GeSi electro-absorption modulators," Nat. Photonics **2**(7), 433–437 (2008).
21. S. Y. Seo, J. Lee, Jung H. E. S. Shin, B. Kang, and S. Bae, "The thermo-optic effect of Si nanocrystals in silicon-rich silicon oxide thin films," Appl. Phys. Lett. **85**, 2526 (2004).
22. R. C. Zaccuri, G. Coppola, and M. Iodice, "Thermo-electro-optical analysis of an integrated waveguide-vanishing-based optical modulator," J. Opt. A: Pure Appl. Opt. **8**(7), S567–S573 (2006).
23. W. M. Green, M. J. Rooks, L. Sekaric, and Y. A. Vlasov, "Ultra-compact, low RF power, 10 Gb/s silicon Mach-Zehnder modulator," Opt. Express **15**(25), 17106–17113 (2007).
24. L. Chen, K. Preston, S. Manipatruni, and M. Lipson, "Integrated GHz silicon photonic interconnect with micrometer-scale modulators and detectors," Opt. Express **17**(17), 15248–15256 (2009).
25. L. Liao, D. Samara-Rubio, M. Morse, A. Liu, D. Hodge, D. Rubin, U. D. Keil, and T. Franck, "High speed silicon Mach-Zehnder modulator," Opt. Express **13**(8), 3129–3135 (2005).
26. G. T. Reed, G. Mashanovich, F. Y. Gardes, and D. J. Thomson, "Silicon optical modulators," Nat. Photonics **4**(8), 518–526 (2010).
27. A. Liu, R. Jones, L. Liao, D. Samara-Rubio, D. Rubin, O. Cohen, R. Nicolaescu, and M. Paniccia, "A high-speed silicon optical modulator based on a metal-oxide-semiconductor capacitor," Nature **427**(6975), 615–618 (2004).
28. A. Anopchenko, A. Marconi, E. Moser, S. Prezioso, M. Wang, L. Pavesi, G. Pucker, and P. Bellutti, "Low-voltage onset of electroluminescence in nanocrystalline-Si/SiO2 multilayers," J. Appl. Phys. **106**, 033104 (2009).

1. Introduction

On-chip integration of photonic devices using CMOS manufacturing tools has become an appealing perspective in the last years [1, 2]. Many encouraging work has heralded silicon photonics as a suitable platform to develop photonic integrated circuits (PIC) that can compete within the aggressive performance and cost demands of short scale telecommunications market [3]. Of particular interest are Er^{3+} doped light emitting devices due to their potentiality as a signal source or amplifier for the C-band at 1.53 μm [4]. Silicon photonics technology has already established platforms in which are possible to integrate low-loss waveguides, electro-optical modulators, switching devices, multiplexers and even detectors [3, 5, 6]. However, all of them lessen if considering architectures suitable for electrical injection and light confinement simultaneously, as the required electrical contacts and the thin film configuration may compromise the effective confinement of the structure. Recently, the slot waveguide configuration was proposed as an alternative geometry able to solve these drawbacks, yielding good mode confinement in a very thin layer with low refractive index [7]. To this end, several work investigated on the optical and electrical properties of slot waveguides, showing promising characteristics for their implementation as functional building blocks [8, 9]. Active slot waveguides where light can be generated and simultaneously coupled to the rest of the photonic circuit were successfully designed [10] and fabricated [11] recently. Er^{3+} doped Si-rich oxide (SRO) was used as a slot layer to yield good injection efficiency and high electroluminescence (EL) performance. Also, much attention has been paid to carrier absorption (CA) losses at 1.53 μm in Si-nanocrystal (Si-ncs) waveguides by means of optical pumping [12], determining an accurate characterization of the optical losses even in slot waveguides [13]. Still, the possible performance of this

#175955 - $15.00 USD Received 11 Sep 2012; revised 30 Oct 2012; accepted 1 Nov 2012; published 12 Dec 2012

geometry in an electrical pump & probe scenario have only been modeled [14], but never studied experimentally.

In this work we report the optoelectronic characteristics and the results of an electrical pump & probe study of Er^{3+} doped Si-based light emitting slot waveguides. Two different active slot waveguides were studied. An Er^{3+} doped oxide (SiO_2) layer was compared with an Er^{3+} doped SiO_2 containing Si-ncs. Such measurements were performed in order to quantify the injected CA losses inside the structure and to investigate on the signal enhancement of the probe signal at 1.53 μm. Finally a plausible modulation scheme in a 1 mm long waveguide is proposed, using the fast dynamics of accumulated carriers at the slot-Si interface in order to modulate the optical signal at competitive frequencies. We obtain an extinction ratio of 6 dB, a spectral bandwidth > 25 nm and a maximum operating power ~120 μW.

2. Device design and setup performance

The Si slot waveguide structure, whose cross section is shown in Fig. 1, was fabricated on silicon on insulator (SOI) wafer. It consists of a thin Er^{3+} doped active layer (SiO_2 or SRO) 40 nm thick, embedded between two Si slabs (horizontal configuration). The preferred deposition techniques for the active layer were low-pressure chemical vapor deposition (LPCVD) for the SRO (with a nominal Si excess of 11.5%) or high temperature oxidization for the SiO_2. The crystalline silicon of the SOI wafer was used as a bottom slab, while the top slab was obtained by a polycrystalline silicon layer which is 100 nm thick and is used both as slab for the waveguide and as an electrode for current injection. N-type doping with a maximum of 10^{19} at./cm^3 was defined at the sides of the polysilicon, remaining the central part undoped. Similarly, using a self alignment method with the specific annealing of the structure, a graded p-type doping profile was defined for the bottom crystalline silicon with an increasing doping concentration that starts near the active layer (10^{17} at./cm^3) down to the bottom electrode with a nominal value of 10^{19} at./cm^3 (see the device cross-section on top of Fig. 1). The bottom electrode (90 nm thick) was 10^{20} at./cm^3 p-type doped. Deep ultraviolet (DUV) lithography was used to define 1 μm wide (x-axis) and 1 mm long waveguides (in z-direction). The structure is cladded by a stoichiometric high temperature oxide (HTO). Finally, vias were etched down to the doped part of the waveguides and Al metal electrodes were formed (see ref. [11]). An optical mode confinement factor of 40% was calculated, defined as the ratio of the optical power in the slot and the total optical power [15].

The total footprint of the active structure is 29 μm wide (along the x-direction), 0.46 μm thick (y-axis) and 1mm long (z-axis). Figure 1 (top panel) shows the waveguide cross-section. The active waveguide is coupled from both facets to a passive slot Si waveguide by means of a slot taper. The latter structure presents an initial width of 1 μm (x-axis), which matches the width of the active waveguide, a length of 800 μm (z-axis) and a final width of 12 μm (passive Si waveguide width). The waveguide cross-section is the same for both taper and active region, except for the top and bottom electrodes, the p-type graded implantation in the lower slab and the Er^{3+} implantation. Figure 1 (bottom panel) shows a top schematic view of the active waveguide-taper-passive waveguide system.

#175955 - $15.00 USD Received 11 Sep 2012; revised 30 Oct 2012; accepted 1 Nov 2012; published 12 Dec 2012

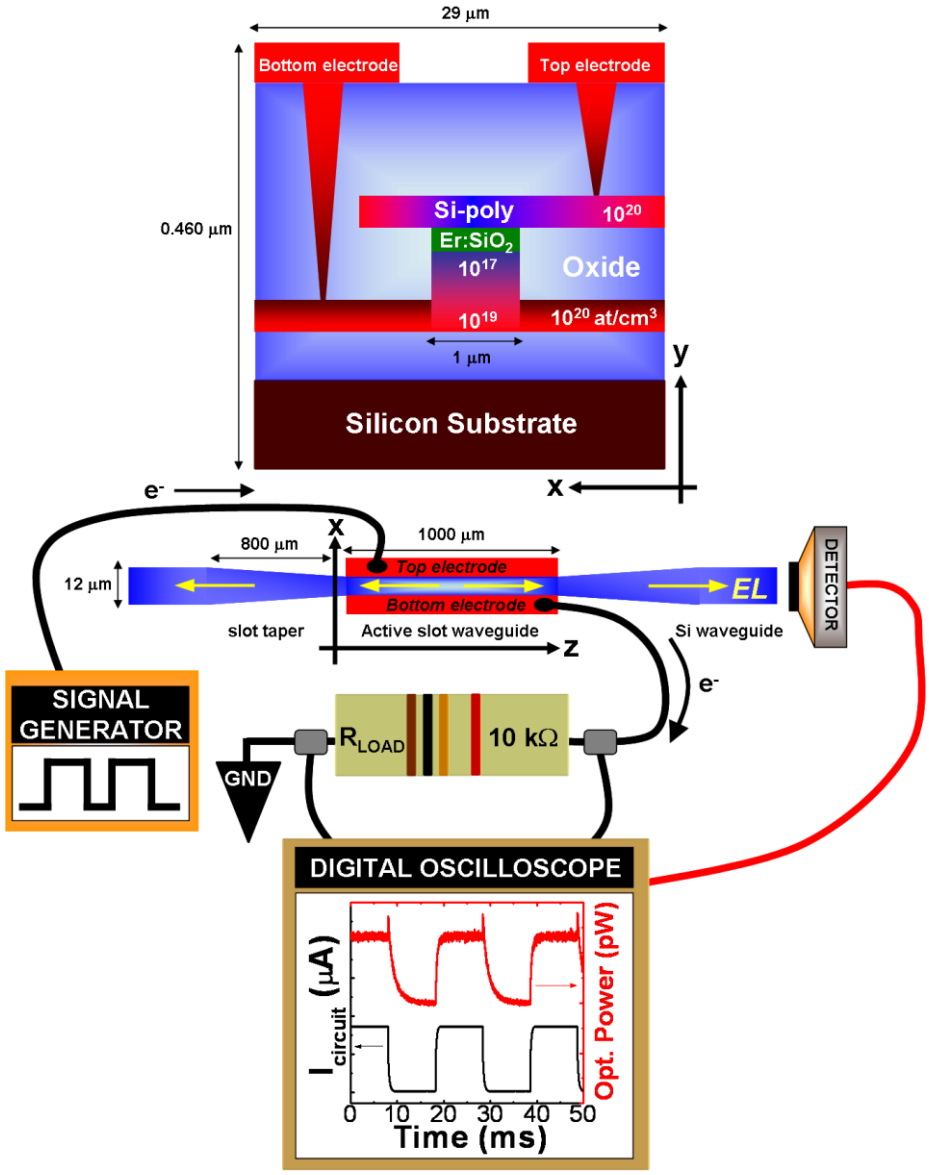

Fig. 1. Slot waveguide cross-section (top panel) and top schematic view (bottom panel) of the integrated system with the experimental configuration used for the measurements. A coordinate system (crossed arrows) is shown to facilitate a spatial view of the waveguides.

The waveguides are excited by a square wave pulse produced by a signal generator (Agilent 8114A), which is directly linked to the top electrode of the waveguide. A load resistance (10 kΩ) is connected in series with the bottom electrode and used to monitor the injected current (see Fig. 1, bottom panel). Simultaneously, the output EL emission at 1528 nm is collected from the waveguide facet by a PMT detector (H10330-25) interfaced with a monochromator with a spectral resolution of 0.1 nm. Both the injected current in the waveguide and the generated EL are monitored through a digital oscilloscope (Agilent DSO 8064A).

Electrical pump & probe measurements were also performed by coupling an infrared laser-diode with a maximum power at 1528 nm (Thorlabs FPL 1009P) in the slot waveguides by means of an output coupler (see ref. [11] for further details). An infrared camera

#175955 - $15.00 USD Received 11 Sep 2012; revised 30 Oct 2012; accepted 1 Nov 2012; published 12 Dec 2012

(Hamamatsu c2741) was used to monitor the guided mode at the output of the waveguide and ensure its good confinement. A pin-hole was also placed before the detection stage to solely select the guided light. Once the probe alignment and detection is optimized, the electric pump is switched on (square wave pulse), and the output signal is recorded.

3. Experimental results

J(V) curves were obtained under negative voltages (accumulation) up to the device breakdown (between −47 V and −48 V) with a quasi-static step voltage of 10 mV/s. Figure 2(a) shows the data, including the range of voltages (from −25 V up to the breakdown) where one single transport mechanism can be identified (Fowler-Nordheim, FN injection). A decrease of the tunneling barrier height was observed when the Si-ncs are embedded, facilitating the electrical injection (higher currents are obtained for the Er:Si-ncs layer) and improving the reliability and device lifetime [16]. Under FN injection, infrared EL was emitted, indicating that the main excitation mechanism is direct impact excitation of the Er ions via the hot carriers injected in the active layer. The characteristic Er emission spectra were observed for the two waveguides (see Fig. 2(b)). Bearing in mind that the spectral resolution of our setup is 0.1 nm, the evolution of the EL spectrum was studied as a function of the applied voltage amplitude revealing no modification of the spectra with increasing voltage, nor any spectral narrowing effects.

A time-resolved characterization of the EL and of the injected current was performed. An example is shown within the digital oscilloscope of Fig. 1 (bottom panel). A clear EL overshoot is observed when the pump voltage is switched off (top signal), which is not correlated with the injected current since no overshoot is observed on the bottom signal.

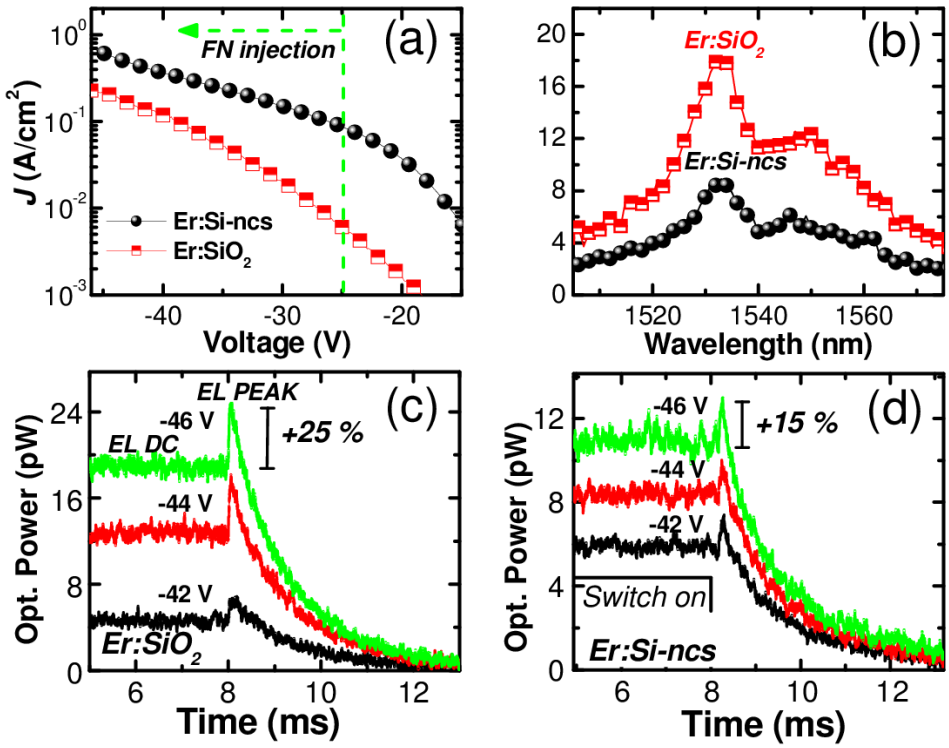

Fig. 2. (a) *J(V)* characteristics of the waveguides under accumulation. (b) EL spectra of both layers obtained under a square wave pulse (V_{pp} = −44 V). (c and d) Time-resolved EL measurements at 1528 nm of the Er:SiO_2 (c) and the Er:Si-ncs (d) slot waveguides as a function of the voltage polarization in the top electrode.

#175955 - $15.00 USD Received 11 Sep 2012; revised 30 Oct 2012; accepted 1 Nov 2012; published 12 Dec 2012

Notice that this feature is not typical for Er^{3+} doped capacitors [17]. Moreover, such an EL peak can be observed in both active waveguides for a voltage range where EL signal is present, until the device breakdown (see Fig. 2(c) and Fig. 2(d)). For comparison, time-resolved EL was also collected from the top of the waveguide (the EL passing through the top polysilicon electrode), but no EL overshoot was observed at any voltage (not shown). From now on, the EL obtained under a constant pump voltage has been labeled as EL_{DC} and the EL overshoot as EL_{PEAK}. Defining the EL relative increase (Δ_{EL}) as:

$$\Delta_{EL}(\%) = \frac{EL_{PEAK} - EL_{DC}}{EL_{DC}} \cdot 100 \quad (1)$$

A value of 25% (15%) is obtained for the Er:SiO_2 (Er:Si-ncs) waveguide. In order to further investigate the origin and evolution of this peak, both EL_{DC} and EL_{PEAK} values were studied as a function of the injected current in several waveguides. For that, the pump voltage polarization was swept from −41 V to −46 V (from EL onset upwards) with a step voltage of 0.5 V. A superlinear increase of EL_{DC} and EL_{PEAK} as a function of the injected current is reported in Fig. 3(a). A power law fit yields exponent of 2.62 ± 0.08 for the EL_{PEAK} and 2.71 ± 0.07 for the EL_{DC} for an Er:SiO_2 waveguide; lower exponents of 2 (in average) are observed for the Er:Si-ncs waveguide (not shown). In addition, almost identical superlinear slope was identified in the $EL_{DC}(J)$ characteristic collected from the top of the waveguide. The lightly doped top polysilicon is thought to be the origin of superlinearity since is the only difference (in terms of cross-section) between our waveguides and light emitting MOS capacitors [17]. A plausible explanation would be that at low voltages the distributed electric field along the top polysilicon is not equipotential because of the non-doped central region. Therefore, the Er^{3+} excitation would take place at the side of the top polysilicon where the top electrode is contacted (see Fig. 1). Increasing the applied voltage would spread the electric field across the top polysilicon, also expanding the effective excitation active area. The exponent difference shown between Er:SiO_2 and Er:Si-ncs waveguides is attributed to a higher barrier height for the former that provides better hot carrier acceleration (then a faster growth of the EL). Therefore, neither the EL_{DC} nor the EL_{peak} are related to an amplifying process inside the waveguides (amplified spontaneous emission, ASE). Furthermore, additional measurements in waveguides with different lengths (1.5 mm, 2 mm, 2.5 mm and 3 mm), showed no dependence between the EL and the waveguide length; the same optical power and similar exponents were obtained in all the waveguides. This behavior was attributed to the on-chip propagation losses which account to 40 dB/cm and prevent photons generated at a distance longer than 1 mm to reach the waveguide facet. Additionally, an EL saturation at high current injection is observed in Fig. 3(a), suggesting either a saturation of the excitable Er^{3+} fraction or the onset of device breakdown (i. e. appearance of additional current pathways that do not contribute to the Er^{3+} excitation). The analysis of the rise (τ_{rise}) and decay (τ_{decay}) times yields single exponential decays (Fig. 3(b)). The following functions were used to extract the characteristic times from the experimental data:

$$EL_{off}(t) = EL_{peak} \cdot e^{-\frac{t}{\tau_{decay}}} \quad (2)$$

$$EL_{on}(t) = EL_{DC}\left\{1 - e^{-\frac{t}{\tau_{rise}}}\right\} \quad (3)$$

A decay time of 1.7 ms which is independent on the injected current was obtained for the Er:SiO_2 waveguide (1.2 ms for the Er:Si-ncs). On the contrary, a strong injected current dependence was observed for the rise time in both waveguides which varies from 1.6 ms (small injected currents) to 0.18 ms (large injected current). From these values and assuming a simple two level model, an injection excitation cross-section σ of the Er^{3+} ions of ~1×10^{-14} cm^2 was found. Notice that this value fits with the one reported for Er^{3+} doped silicon

#175955 - $15.00 USD Received 11 Sep 2012; revised 30 Oct 2012; accepted 1 Nov 2012; published 12 Dec 2012

dioxides [18]. An upper injection CA lifetime of 10 μs was also measured, equal to our time circuit constant (τ_{RC} ~*10 μs*). Nevertheless, lower CA lifetimes (in the order of few ns) are expected in our devices for an optimized experimental setup (with lower τ_{RC}) [19].

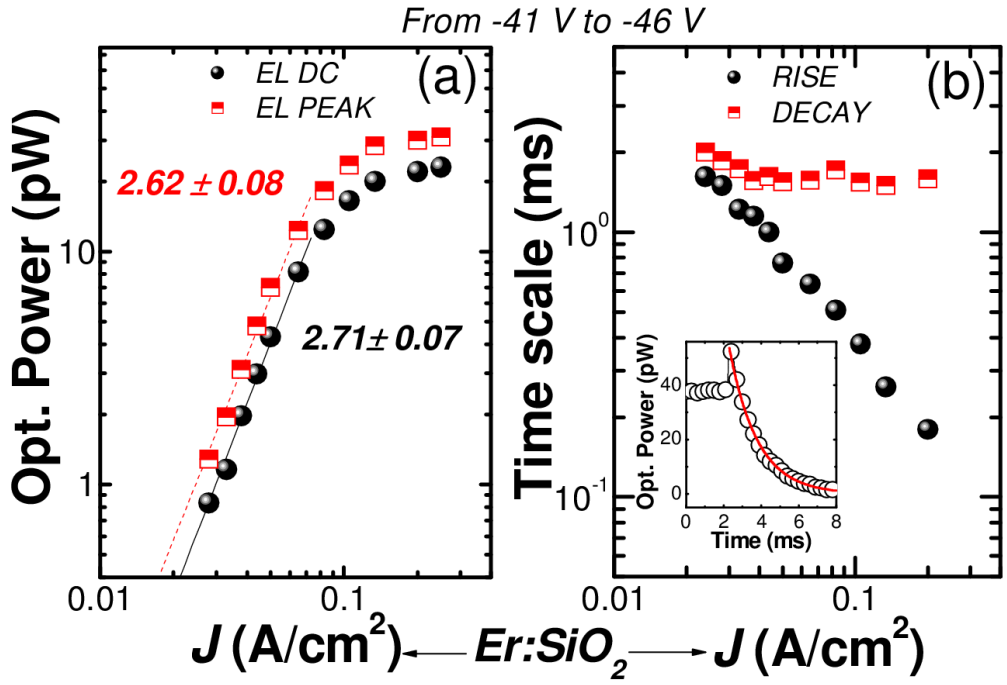

Fig. 3. (a) Intensity of the DC and peak EL value as a function of the injected current density for the two waveguides studied. (b) Decay (half filled squares) and rise (circles) times as a function of the injected current. The inset shows an example of a decay fit of the experimental data. This figure shows a representative measurement in an Er:SiO_2 waveguide.

Disregarding stimulated emission, the sharp EL_{PEAK} can be explained by taking into account two independent mechanisms: The excited Er recombination dynamics and the CA dynamics. When the pump voltage is switched on, additional optical losses (superimposed to the propagation losses, α_{prop}) are generated due to the injected carriers (CA losses). When the pump is turned off, the injected carriers recombine. Carrier recombination reduces the waveguide losses to α_{prop}, and since the Er^{3+} lifetime is long, an increase of the EL signal is observed. This explains the EL_{PEAK}. The difference in the EL_{PEAK} value in the two waveguides suggests carrier trapping within the active waveguide due to the Si-ncs.

Further insight comes from time-resolved electrical pump & probe measurements. A continuous probe signal at 1528 nm was coupled to the waveguide with a power comparable to the EL signal. This is done in order to work on the low signal gain regime, where the probe signal does not modify the population of the levels. Then, a square voltage signal (0 to negative value) with a frequency of 50 Hz is used as a pump source. The different panels of Fig. 4 show the evolution of the EL (I_{EL}, black curves at the bottom) and of the transmitted probe signals ($I_{p\&p}$, red curves on top) for different pump voltages within a voltage interval where I_{EL} is detectable. For clarity, it has been identified the time window in which only the probe signal is propagating and the pump is switched off (indicated by *p-off*), and also the one in which the pump is activated (*p-on*). It is clear that, within the *p-on* region, $I_{p\&p}$ gets strongly attenuated with respect to the *p-off* region and reaches the I_{EL} level for pump voltages of −44 V (and above). In particular, in the *p-off* region at −42 V, a small overshoot contribution in $I_{p\&p}$ is observed during the first milliseconds. This contribution becomes a sharp peak for higher pump voltages. However, it essentially reproduces the temporal behavior observed in the I_{EL} dynamics (black line) already discussed. Thus, $I_{p\&p}$ can be

#175955 - $15.00 USD Received 11 Sep 2012; revised 30 Oct 2012; accepted 1 Nov 2012; published 12 Dec 2012

explained in terms of CA losses, which dramatically quench the probe signal when carrier injection occurs.

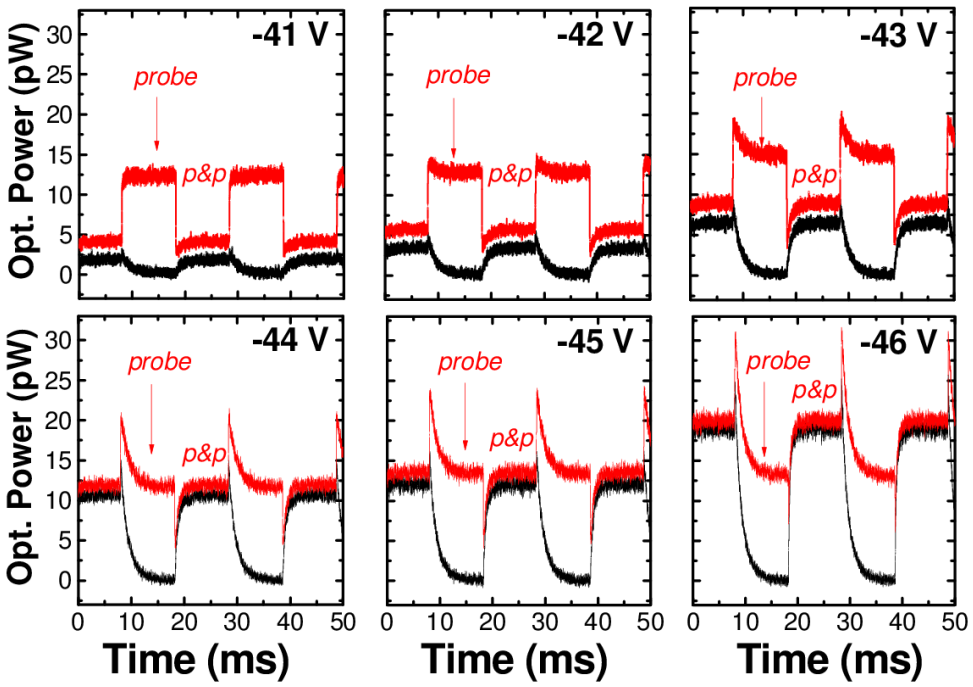

Fig. 4. Electrical pump & probe measurements of an Er:SiO_2 waveguide at 1528 nm (top red line) under square wave electrical bias. Each panel refers to different square wave amplitude. The EL has been also measured for each voltage polarization (black line at the bottom).

To isolate the temporal behavior of the probe transmittance from the EL contribution, the following equation has been applied:

$$Transmittance = \frac{10}{L}\log\left(\frac{I_{p\&p} - I_{EL}}{I_{probe}}\right) \tag{4}$$

where L is the waveguide length and I_{probe} is the asymptotic value of $I_{p\&p}$ during the p-off phase. The transmittance is illustrated on Fig. 5 for the case of the highest voltage amplitude (–46 V).

#175955 - $15.00 USD Received 11 Sep 2012; revised 30 Oct 2012; accepted 1 Nov 2012; published 12 Dec 2012

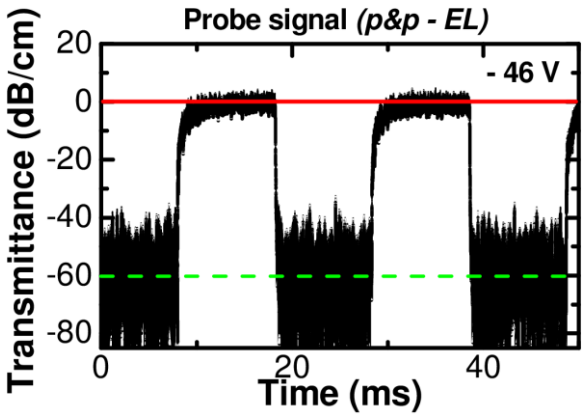

Fig. 5. Transmittance at 1528 nm in the Er:SiO_2 waveguide for a square wave bias of –46 V. This figure was obtained by subtracting the EL signal to the pump & probe measurements of the panel in the right-bottom side of the Fig. 4. The green dashed line marks the average transmittance when the voltage source is on.

It is clearly revealed that no signal enhancement is present (the threshold is marked with a horizontal red line) even within the p-off region, where the injected CA losses are suppressed and the peaks on I_{EL} and $I_{p\&p}$ were evident. During the pumping time, the average injected CA losses can be as high as 60 dB/cm (see the green dashed line in Fig. 5). It is also worth noticing that a slow recovery of the probe signal can be identified when the pump is switched off. Other authors have already observed this phenomenon under optical pumping, and attributed it to a thermal contribution when high pump fluxes are applied [12]. In our devices, the slow recovery time is observed starting at –25 V. This evidences that the waveguides are subjected to a high thermal budget under electrical polarization.

Finally, an additional pump & probe approach was carried out by modulating simultaneously the probe signal (200 kHz) and the voltage source (10 Hz). In that case, a lock-in technique in combination with a time-resolved configuration was used. The lock-in amplifier locked on the probe beam transmission, and its output signal monitored by the oscilloscope which was triggered by the voltage source. This way the modulation depth caused by the injected CA losses was carefully monitored, since the EL is filtered out by the lock-in. The square wave voltage amplitude was changed from 0 to –45 V, with a step voltage of 2.5 V. Results are shown in Fig. 6, where the time-resolved transmittance of a probe beam at 1528 nm (Fig. 6(a)) and the spectral transmittance (Fig. 6(b)) are characterized under different amplitude voltages. The probe signal is strongly attenuated under injection, and becomes more evident as the square wave voltage increases. Notice that no spectral dependence of the attenuation (Fig. 6(b)) is observed at any voltage for probe beam wavelengths from 1515 nm to 1540 nm, i.e. over a 25 nm interval.

#175955 - $15.00 USD Received 11 Sep 2012; revised 30 Oct 2012; accepted 1 Nov 2012; published 12 Dec 2012

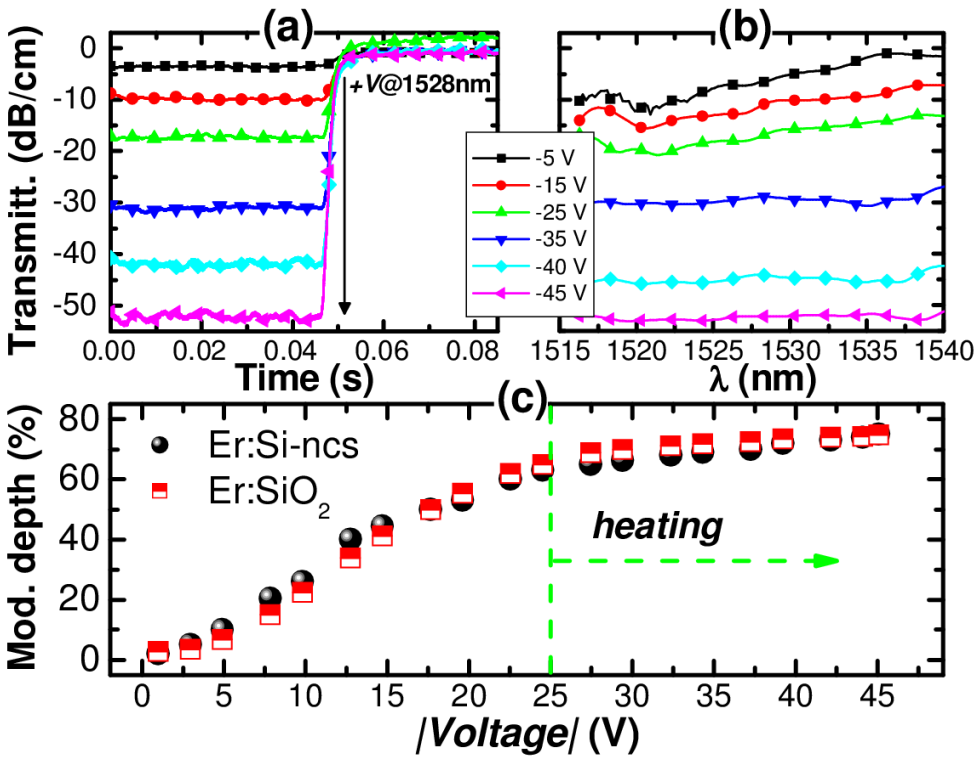

Fig. 6. (a) Time-resolved probe intensity transmittance at 1528 nm and (b) spectral transmittance for different voltages (given in the legend) and for the Er:SiO_2 waveguide. (c) Modulation depth as a function of the applied voltage for the two waveguides. The green dashed line indicates the threshold where heating effects start to be sizable.

Figure 6(c) shows the voltage dependence of the modulation depth (η) of the transmission beam. This represents the contribution of the injected CA as a function of the applied voltage for the two waveguides under study. The following equation was used [20]:

$$\eta(\%) = [1 - \exp(-\Delta\alpha(V)L)] \cdot 100 \qquad (5)$$

where $\Delta\alpha(V)$ is the loss variation due to the applied bias. A linear trend is obtained for applied voltages < 25 V, then triggering a regime in which the modulation depth tends to saturate (from 25 V and above). Notice that this voltage coincides with the FN injection onset. Also, considerable heating of the waveguide is expected under these medium-high pump voltages (see the slow recovery time of the probe signal in Fig. 5). Heating affects the refractive index and, hence, promotes the optical mode delocalization which, in turn, induces the saturation of the modulation depth [21, 22]. On the contrary, a rather different condition prevails for voltages below the tunnel injection threshold (25 V). In that case, negligible CA contribution due to the injected current across the slot layer is predicted (the current being ~*nA*). Carriers are mainly accumulated at the slot interface when the polarization is switched on. Therefore, the heating is reduced while modulation can be achieved. A maximum modulation depth of 75% is observed in both waveguides, which corresponds to an absolute extinction ratio of 6 dB in our 1 mm long waveguides. Notice that the inclusion of Si-ncs does not improve the modulation capabilities of our waveguides.

Since this value is comparable with that of d.c. based pn junction silicon modulators [23, 24], it is interesting to analyze our 1 mm long waveguides as potential candidates as integrated electro-optical modulators. Measured propagation losses are almost 4 dB, a value which is lower than the ones of Mach-Zehnder (MZ) optical modulators [25]. The length is 1 mm which is also shorter than the one of MZ modulators and yields a lower footprint in the

#175955 - $15.00 USD Received 11 Sep 2012; revised 30 Oct 2012; accepted 1 Nov 2012; published 12 Dec 2012

photonic chip. In addition, although the voltage needed for a 6 dB modulation is quite high (~40 V) and introduces some heating, the current remains very low (~3 μA), providing d.c. operational power of 120 μW which is a competitive value for silicon modulators [26]. The spectral bandwidth (minimum of 25 nm, see Fig. 6(b)) is wider and the thermal stability is better with respect to ring resonator or MZ based modulators, which rely on the interferometry. Though not demonstrated here, a modulation speed > 1 GHz is foreseen by using the accumulation of carriers at the interface as considered in previous work [27]. Then, assuming a modulation speed of 1GHz, the estimated energy per bit would be around of 120 $fJ \cdot bit^{-1}$ similar to that of the most efficient modulators [24]. Therefore, all the presented characteristics can be used to develop a robust electro-optical modulator with the slot layer entirely formed by a SiO_2 only (with no Er implantation neither Si-ncs). Also, an active waveguide modulator can be anticipated if using Er-doped SiO_2 waveguides. In that case, monomodal EL at 1.53 μm would be generated in the waveguide and directly modulated avoiding the on-chip coupling of an external laser (the light source and the modulator would be integrated within a single silicon photonic chip). A remarkable improvement of the optoelectronic characteristics is expected in slot waveguide modulators when optimization of the top electrode is performed. A more accurate doping distribution and a multilayer structure of SiO_2 and silicon-rich oxide (SRO) in the slot can be also engineered to reduce the onset voltage required for the modulation [28].

4. Conclusions

An injection voltage dependent study of Er^{3+} doped slot waveguides have been performed to quantify the injected carrier induced losses. The Er^{3+} electroluminescence has been characterized at 1.53 μm for two different active materials (Er^{3+} doped SiO_2 or Si-rich oxide) in the slot region of the waveguides. In time-resolved experiments, we obtain a sharp EL peak when the voltage is switched off due to the different lifetimes of excited Er^{3+} ions and of the generated carriers. An electrical pump & probe measurement has allowed us to determine the injected carrier losses in 1 mm long waveguides, obtaining an extinction ratio in d.c. modulation of 6 dB with an operation power consumption of 120 μW and a spectral bandwidth > 25 nm. Further improvements in terms of power consumption can be considered if the top electrode, the active slot layer and the doping distribution are optimized.

Acknowledgments

This work was supported by the Spanish Ministry of Science through the project LASSI (TEC2009-08359), and by the EC through the project ICT-FP7-224312 HELIOS and by Italy-Spain integrated actions. The authors thank Alessandro Marconi and Olivier Jambois for contributions at an early stage of this work.

#175955 - $15.00 USD Received 11 Sep 2012; revised 30 Oct 2012; accepted 1 Nov 2012; published 12 Dec 2012